RT E JOURNAL

Fused filament fabrication (FFF) of bio-based low-density polymer foams

Jonas Fischer[a] (ORCID iD: 0000-0001-7296-9644), Lisa Heinecke[a], Patrick Springer[a] (ORCID iD: 0000-0001-7181-0148), Moritz Becker[b], Benedikt Bitzer[b]

[a] Fraunhofer Institute for Manufacturing Engineering and Automation IPA, Stuttgart, Germany

[b] Fraunhofer Institute for Chemical Technology ICT, Pfinztal, Germany

https://doi.org/10.58134/fh-aachen-rte_2024_006

Zusammenfassung In einer Welt, in der der Leichtbau aufgrund der Notwendigkeit, Ressourcen zu schonen und die Treibhausgasemissionen zu senken, eine immer wichtigere Rolle spielt, ist es wichtig, neue Technologien zu entwickeln, die leichtere Produkte ermöglichen. Die additive Fertigung bietet aufgrund ihrer Gestaltungsfreiheit ein hohes Leichtbaupotenzial durch die Realisierung niedriger Bauteildichten, aber es ist noch nicht möglich, Polymerschäume mit niedriger Dichte zu drucken, um noch leichtere Teile zu erhalten. Daher wird in diesem Beitrag ein neuartiges, extrusionsbasiertes additives Fertigungsverfahren vorgestellt, bei dem ein biobasiertes Polymerfilament mit einem physikalischen Treibmittel zur Herstellung von Schaumteilen verwendet wird. Ein Extrusionsversuchsaufbau ermöglicht die Analyse der Randbedingungen der Schaumextrusion, d. h. der Beziehung zwischen Vorschubgeschwindigkeit, Heiztemperatur, Durchmesser des extrudierten Materials, Extrusionskraft und Dichte des extrudierten Materials. Niedrigste Dichten lassen sich durch niedrige Temperaturen und schnellstmögliche Einzugsgeschwindigkeiten bei diesen Temperaturen erreichen. Eine umfassende Parameterstudie zur additiven Fertigung eines einfachen Schaumstofftestteils zeigt durchgängig niedrige Dichten von nahezu 100 kg/m3 bei ausreichender Druckqualität. Die Analyse der Schaummechanismen von drei ausgewählten Szenarien zeigt, dass die verwendete Berechnungsmethode eine ausreichende Vorhersagekraft für die Druckergebnisse besitzt. Mit der verwendeten Charakterisierung lassen sich Korrelationen der Expansionsgeschwindigkeit und -zeit des Polymers während des Drucks nach dem Druckprozess recht gut abbilden.

Abstract In a world in which lightweight construction is playing an increasingly important role due to the need to conserve resources and lower the greenhouse gas emissions, it is important to develop new technologies that enable lighter products. Additive manufacturing offers a high lightweight potential due to its freedom of design by realising low part densities, but it is not yet possible to print low-density polymer foams to achieve even lighter parts. Therefore, this paper presents a novel, extrusion-based additive manufacturing process that uses a bio-based polymer filament loaded with a physical blowing agent to manufacture foam parts. An extrusion test setup allows the analysis of foam extrusion boundary conditions, i.e. the relationship between feeding velocity, heater temperature, extruded material diameter, extrusion force and extruded material density. Lowest densities can be achieved by using low temperatures and fastest at this

temperature possible feeding velocities. A comprehensive parameter study on the additive manufacturing of a simple foam test part shows continuous low densities of nearly 100 kg/m^3 with an adequate print quality. The analysis of the foam mechanisms of three selected scenarios demonstrates that the calculation method used has adequate predictive power for print results. With the characterisation used, correlations of the expansion velocity and time of the polymer while printing can be reasonably well mapped after the printing process.

Introduction and motivation

Conserving resources is an increasingly important task due to the increasing concentration of greenhouse gases in the earth's atmosphere. Fossil-based polymers in particular cause high greenhouse gas emissions, not only through their production and disposal, but also during their transport. The production part can be reduced by using recycled materials [1] or bio-based polymers [2], while the transport share can be achieved by reducing the mass of the transported products. Polymer foams can enable low masses due to their low density, but are currently often fossil-based [3] and are sometimes produced in simple moulds and then individualised by machining [4]. Additive manufacturing can enable individualisation and thus contribute to further resource conservation. This effect can be enhanced by using bio-based plastics.

Definitions

Additive manufacturing is a potentially well-suited manufacturing process for the production of polymer foam components due to its freedom of design. This is reflected in the number of foaming processes already described in the literature. A good overview is provided by Nofar et al. [5], who identified four main methods: 1) Construction of porous structures (lattice structures) [6, 7]; 2) Syntactic foaming [8–10]; 3) Post-foaming of pre-moulded solid foams [11, 12]; 4) In-situ foaming of filaments loaded with blowing agents [13–15]. The additive manufacturing of lattice structures is an established process that only enables macroscopically porous structures, i.e. no micropores and therefore no intrinsic density reduction. Syntactic foaming and post-foaming require a pre-process to insert the fillers and a post-process to remove the fillers respectively for subsequent foaming. All of the process variants mentioned enable a lower density than the bulk material down to a minimum density of approx. 300 kg/m^3 [9] of the additively manufactured components. In conventional production, densities up to ten times lower can be achieved with a thermoplastic polylactide (PLA) [16]. In the following, the in-situ foaming of filaments loaded with blowing with the aim of achieving an adequately low density of produced parts will be discussed.

Method

This paper presents a fused filament fabrication (FFF) process that enables the processing of filaments loaded with a physical blowing agent. Figure 1 shows the process used in this approach schematically. After the thermoplastic filament has been produced, it is loaded with a gaseous blowing agent. After transport and storage, the loaded filament is processed using an FFF printer to produce a foam component.

The manufacturing process is simplified according to the principle of mass conservation.

$$\sum_{i=1}^{n} \dot{m}_i = \sum_{i=1}^{n} \rho_i \cdot \dot{V}_i = \sum_{i=1}^{n} \rho_i \cdot v_i \cdot A_i = 0 \quad (1)$$

The sum of the mass flows $\dot{m}_i$ and the volume flows $\dot{V}_i$, which depend on the densities ρ_i,

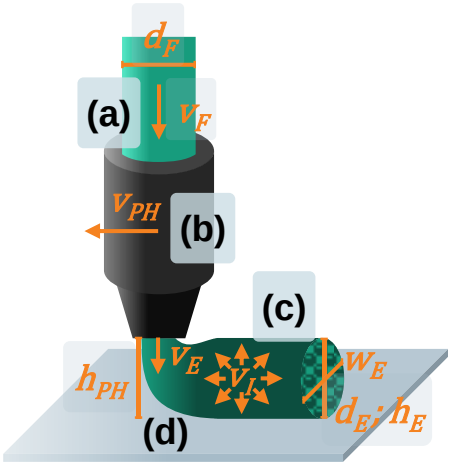

Figure 2: Schematic view of material deposition: (a) filament; (b) hotend; (c) deposited foam material; (d) print bed

is 0. The conditions in an FFF process are shown in Figure 2.

By considering the hotend as a flow system, the following assumption can be made, neglecting thermal effects.

$$\rho_F \cdot v_F \cdot A_F = \rho_E \cdot v_E \cdot A_E \quad (2)$$

Here, ρ_F is the density, A_F the cross-sectional area of the filament and v_F the feeding velocity as well as ρ_E the density, A_E the cross-sectional area of the extruded material and v_E the velocity of the material at the nozzle outlet.

Comminal et al. [17] simulated possible cross-sectional areas of the deposited strand – in this case the cross-sectional area of the extruded material A_E – taking into account thermal effects for bulk material in the FFF and found that these depend on the print head height

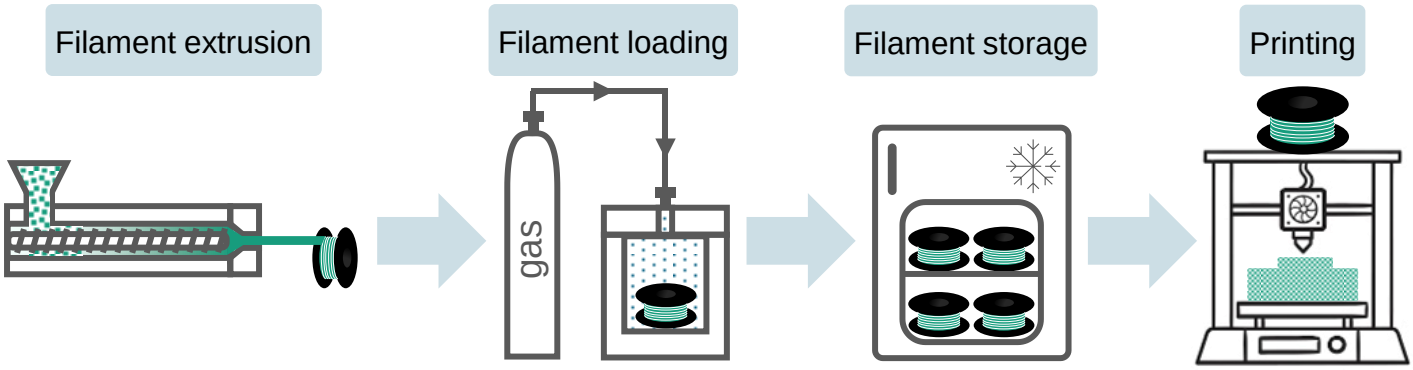

Figure 1: Foam printing process: from filament extrusion and loading over storage to printing

or layer height h_{PH}. The lower the print head height, the more the geometry of the cross-

sectional area changes from a round circle to a cuboid with rounded corners. This must be taken into account in the calculation. As a low h_{PH} leads to compressive forces on the already formed foam, this could compact the deposited material in the still lower viscous, soft state and increase the density of the extruded material ρ_E undesirably. For a circular cross-section, the following relationship is assumed with d_F, the diameter of the filament and d_E, the diameter of the extruded material.

$$\rho_F \cdot v_F \cdot \frac{{d_F}^2 \cdot \pi}{4} = \rho_E \cdot v_E \cdot \frac{{d_E}^2 \cdot \pi}{4} \tag{3}$$

When printing with solid material, the print head velocity v_{PH} is often calculated on the assumption that the processing material is an incompressible fluid. As the extruded cross-sectional area A_E does not always correspond to the geometry specified in the printer's control system calculation model and the material is not always

completely incompressible, a multiplier M is used to compensate for these effects, which cannot be predicted exactly. Depending on the cross-section under consideration, the continuity equation is used, whereby h_E is often also regarded as the height of the extruded material and w_E is the width of the extruded material.

Circle: $$v_F \cdot \frac{{d_F}^2 \cdot \pi}{4} = v_{PH} \frac{{d_E}^2 \cdot \pi}{4} \cdot M$$

Rectangle: $$v_F \cdot \frac{{d_F}^2 \cdot \pi}{4} = v_{PH} \cdot h_E \cdot w_E \cdot M \tag{4}$$

In FFF with thermoplastic foam, a further factor, the internal expansion velocity of the material v_I, must be taken into account. Depending on when the expansion takes place and in which direction a free expansion of the material is possible, v_{PH} can have an increasing or decreasing effect on the extruded material density. It is assumed that the time of expansion of the material is primarily triggered by the temperature of the material and the surrounding pressure. As hotends are not currently designed to be gas-tight, gaseous blowing agents can leak. It can also be assumed that the foaming process already begins in the hotend in some cases. If the material expands immediately after exiting the nozzle, it has free space if $v_{PH} \geq v_I$. This should be the ideal case. If $v_{PH} < v_I$, only d_E or w_E may increase due to the lack of free volume in the print direction and in the direction of the print head. If the expansion takes place later, d_E or w_E and simultaneously h_E can become larger, as the upward-limiting print head has already moved away. The requirement for this is that the molten material at this point has a sufficiently high temperature and the viscosity is low enough to allow pore growth. Ideally, the temperature of the material will have dropped to such an extent by the time pore growth is complete that the increased viscosity of the material prevents the structure from shrinking. The material should therefore cool down as quickly as possible after leaving the nozzle and expansion in order to achieve a minimum density ρ_E in the extruded strand.

The tests were carried out in a two-step approach. (1) Free-flow extrusion tests were carried out as a function of the heater temperature T_H and the feeding velocity v_F in order to classify the extrudability of the material. At the same time, the extrusion force F_E was recorded. The diameter d_E and the density of the extruded material ρ_E were measured at room temperature. (2) Single-path tower samples with an edge length of 50 mm and a height of 16 mm were printed in an FFF printer using the suitable parameters found. The heating element temperature T_H, the feeding velocity v_F, print head velocity v_{PH}, multiplier M and additionally the print head height h_{PH} were varied.

Materials

The material used in this work is a blend of different PLA types from the "Luminy® PLA" portfolio of "TotalEnergies Corbion". Specifically, the types "L175" and "LX975" were used. These PLA types differ mainly in the L-isomer content and thus in the crystallinity. The "L175" has an L-isomer content of ≥ 99 % and has the highest crystallinity of the materials used. The "LX975" has an L-isomer content of 88 % and is completely amorphous. The crystallinity plays an important role both for gas absorption and for the subsequent foaming process in the printer. The only additive used was 0.5 % "Talc L88" as a nucleating agent.

The filaments were extruded on a "HAAKE PolyLab" twin-screw extruder and wound onto a filament spool after cooling in a water bath. The filaments produced are physically loaded with a blowing agent in an autoclave process. The blowing agent used is the gas 1,3,3,3-tetrafluoropropene, which is also known under the trade name "HFO 1234Ze". It was chosen because it has good solubility in PLA. During the loading process, the filaments are placed in the autoclave and exposed to the blowing agent at a selected temperature-pressure-time regime. The pressure results from the vapour pressure of the selected temperature. The amount of gas is selected so that a saturated atmosphere with a constant concentration is created and this remains constant when it is injected into the filament. With this method of loading, blowing agent contents of 10 wt % – 20 wt % can be achieved in the filament. Due to these high blowing agent contents in the polymer compared to foam extrusion [16, 18], a certain proportion of the blowing agent must be present in liquid form in the autoclave in order to fulfil the above-mentioned condition. The exact blowing agent content in the filament depends on the temperature and the saturation time. Maximum saturation is reached after approx. 18 hours at the selected loading temperature. After treatment, the loaded filament is apparently indistinguishable from unloaded filament. However, it is characterised by a greatly increased flexibility compared to the previous state. This flexibility can be explained by the fact that the blowing agent also acts as a plasticiser.

After treatment, it can be observed that the blowing agent content in the filament decreases again over time. This is to be expected, as storage in an air atmosphere corresponds to a reversal of the loading. In order to ensure the longest possible shelf life of the filament, various storage conditions were investigated. With regard to the highest possible blowing agent content over time, storage at < -15 °C is the most favourable. This preserves the blowing agent in a thermodynamically and kinetically favourable way. This means that blowing agent contents of over 10 wt % can be guaranteed even after storage for several months. In this study, the above-mentioned storage conditions were maintained and a processing time of less than two weeks was always achieved, so that a low loss of blowing agent can be assumed.

Experimental setup

An extrusion force measuring setup according to Fischer el al. [19] was initially used to process the filament loaded with blowing agent. This allows the extrusion force to be measured with an annular force sensor inside the hotend. The 3D printer used for the tests is a modified “German RepRap X400” as shown in Figure 3. The loaded filament (a) is fed to the print head via a tubing system and transported towards the hotend with the 0.8 mm nozzle (c) using the feeding unit (b). The printer has a water cooling system for strong thermal separation of the hotend and feeding unit. After exiting the nozzle, the processing material foams and is applied to a heated print bed (d). The printer has an insulated print chamber (e). The control display (f) can be used to start print jobs and monitor the current status of the print. The density measurement was carried out on a precision scale "Precisa LS 220A" according to Archimedes' principle in water. Samples with a mass of 0.1 g were used throughout the material characterisation. The measurement was repeated six times and the mean value was calculated. The microscope images were taken using a "Leica DVM6" optical microscope.

Figure 4: Extruded material sample

Foam extrusion characterisation

Experimental design foam extrusion

Extrusion characterisation is an important tool for determining initial boundary conditions for the FFF process. Filaments with a length of 60 mm were extruded through a nozzle with a diameter of 0.8 mm. The heating element temperature T_H was varied in 10 °C steps from 160 – 230 °C. At the same time, the feeding velocity v_F was changed from 3 – 12 mm/s in steps of 1.5 mm/s. The test plan can be found in Table 1 in the Appendix. The extrusion force F_E was averaged over the measuring length. The diameter of the extruded material d_E was measured at five points on the cooled strand and the average was calculated. The density of the extruded material ρ_E was also determined.

Figure 3: Experimental set-up: (a) filament entrance; (b) filament feeder;(c) hotend; (d) heated print bed; (e) insulated print chamber; (f) control display

Results foam extrusion

Not all parameter combinations allowed the filament to be extruded. Particularly low T_H caused the extrusion to stop at higher v_F. But even high T_H at low v_F had the consequence that the filament buckled immediately after the feeding unit due to the flexibility and an

additional temperature-related loss of stiffness of the filament. An example of an extruded foam strand is shown in Figure 4.

The results of the foam extrusion tests are shown in Figure 5. With increasing v_F, d_E increases until it levels off at approx. d_E = 1.8 mm after a maximum of d_E = 2.2 mm. The density ρ_E shows a strong temperature dependence at v_F = 3 mm/s and is smaller at lower T_H. The higher v_F becomes, the higher ρ_E becomes. The lowest density of ρ_E = 99.8 kg/m³ was achieved at v_F = 4.5 mm/s and T_H = 180 °C. The extrusion force F_E shows a similar behaviour, when v_F is increased. A higher T_H shifts the curve in the direction of lower F_E

Discussion foam extrusion

This analysis shows, that low densities of the extruded material ρ_E of less than 100 kg/m³ can be achieved. With regard to the diameter d_E measured during extrusion characterisation, it is assumed that this is dependent on the temperature of the extruded material and consequently on its viscosity and the cooling time. The longer the material remains in a plasticised state after extrusion, the greater the chance that the material will collapse before d_E is measured and a lower d_E will be measured. This means that ρ_E is also influenced to higher values by a possible collapse of the extruded material. Compensation through faster v_F and thus lower heat input into the material is only possible to a small extent, as the example of the density reduction of approx. 84 kg/m³ at T_H = 230 °C from v_F = 9 mm/s to v_F = 12 mm/s shows. The higher extrusion force F_E measured under these conditions is noticeable, which could be an indication for the assumption of pressure-triggered expansion. Consequently, a low ρ_E is unexpectedly only achieved with a low heater temperature T_H. As a result, only low v_F can be set in order to achieve the lowest ρ_E. Low T_H and high v_F mean, that the filament does not achieve a sufficiently low viscosity and therefore cannot be fed through the nozzle. This can confirm the result of the extrusion force measurement. Stable extrusion with only slightly increasing F_E always occurs at $v_F \leq 6$ mm/s (see Figure 5, green area), which does not always result in a low density. The increasing ρ_E with increasing T_H at v_F = 3 mm/s for example, suggests that due to the low v_F the expansion already takes place primarily inside the hotend and therefore only compacted, molten material emerges from the nozzle.

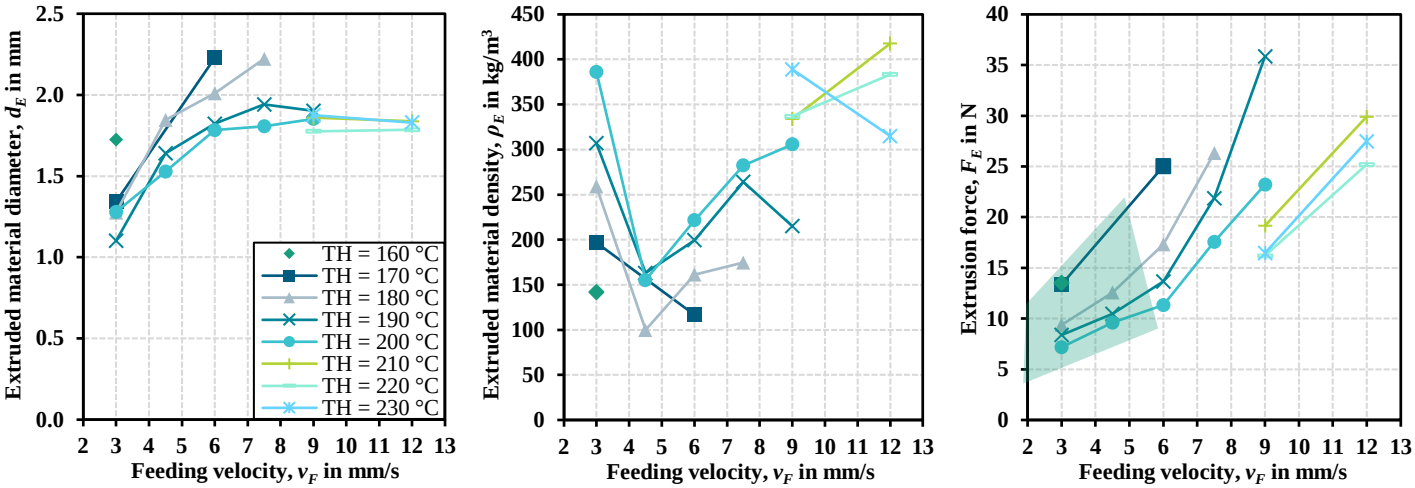

Figure 5: Extrusion characterisation result: extruded material diameter dE (left), extruded material density ρE (middle) and extrusion force FE (right) as functions of feeding velocity vF at different heater temperatures TH

Foam printing

The experimental design of foam production in FFF with a physical blowing agent-loaded filament must be prepared differently than in FFF with bulk material due to the expansion of the material that must be taken into account. A single-path, square geometry (see Figure 6) with a height of H_P was selected as the test specimen and up to four of the test geometries were loaded into the "Simplify3D" software as a slicer for each print job.

A skirt (a) around each test specimen should guarantee sufficient material output from the start of the test specimen print. The first layer (c) was printed at half the print head height (here: layer height) h_{PH}. The heater temperature T_H, the print head velocity v_{PH}, the extrusion width w_E, the print head height (here: layer height) h_{PH} and the multiplier M were identified as the most important variables to be set in the slicer and were specified individually for each test geometry. T_H was varied between 160 °C and 180 °C, starting at 170 °C, based on the findings for the lowest possible density from the extrusion tests. The reason for choosing T_H = 170 °C is that the lowest densities were achieved there for the velocities explained below. Velocities of 25 mm/s to 75 mm/s were selected for v_{PH}. It started with v_{PH} = 50 mm/s. In the path planning, the slicer calculates the required volume of polymer according to the principle of mass conservation described in Eq. (4). However, a rectangular cross-sectional area of the extruded material A_E is assumed here. Since the formation of a circular A_E was assumed here, the extrusion width w_E and the print head height (layer height) h_{PH} were selected as the same in the settings and varied from w_E = 1.49 – 2.15 mm based on the limit diameter from the extrusion tests of $w_E \approx$ 1.9 mm, initially in 0.25 mm steps and later in relative dimensions of 5 % of the initial value. Since the height of the test specimen H_P was specified as constant due to dimensional accuracy, the test specimen had a different number of layers n_L, which can be calculated as follows after subtracting the first layer printed with half the height.

$$n_L \approx \frac{H_P - \frac{h_{PH}}{2}}{h_{PH}} \tag{5}$$

The value was rounded to integer. The multiplier M was calculated by transforming Eq. (4), whereby A_E was assumed to be quadratic and feeding velocities of $v_F \approx$ 4 – 11 mm/s were specified. After conversion, this corresponds approx. to the values of $v_F \approx$ 3 – 9 mm/s for the circular cross-section from the extrusion test, which resulted in a low density. The print bed temperature was set to 60 °C and a thin layer of "Magigoo Original" adhesive was applied to the print bed to improve adhesion. The complete test plan can be found in the Appendix in Table 2. After printing, the actual extrusion width $w_{E,m}$ and the actual height of the test specimen $H_{P,m}$ were measured at three points on each side of the cuboid and the respective mean value was determined. The measured, averaged layer height $h_{E,m}$ was determined after removal of the first layer in accordance with Eq. (5).

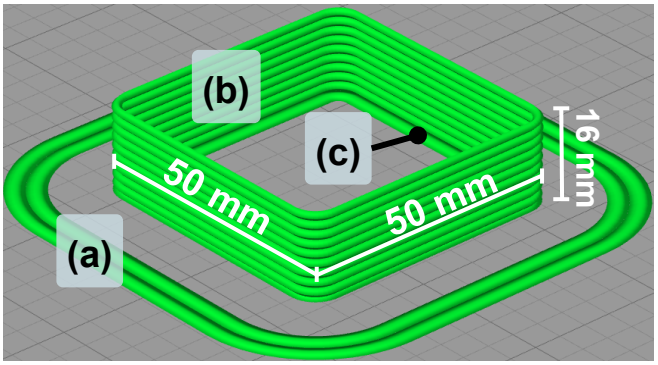

Figure 6: Foam print test part: (a) skirt; (b) layers; (c) first layer

$$h_{E,m} \approx \frac{H_{P,m}-\frac{h_{PH}}{2}}{n_L} = \frac{H_{P,m}-\frac{h_{PH}}{2}}{\frac{H_P-\frac{h_{PH}}{2}}{h_{PH}}} \quad (6)$$

The density ρ_E was measured on each side of the cut samples and the average value was calculated.

Results foam printing

The overall results of the tests are summarised in Table 3 in the Appendix. The first printing tests showed strong fluctuations and there were results with either under-extruded (Figure 7, left) or over-extruded (Figure 7, right) test samples. A total of ten of these results could not be utilised as the material did not adhere to the print bed. A further five test specimens collapsed due to under-extrusion and no clear height of the test specimen $H_{P,m}$ could be determined. In addition, there was a strong influence of the set parameters on each other so that suitable, smaller variation differences had to be found first. An example of an optically good component with a low density ρ_E = 113 kg/m^3 is shown in the centre of Figure 7. A microscopic image of the cross-section of this component can be seen in Figure 8. The pores are larger at the edge of the cross-section than inside. Despite the low density, it can be concluded that the expansion inside the strand is not sufficiently triggered by T_H.

Discussion foam printing

Firstly, a comparative test shows the reproducibility of the results P05, P72, P05, P72, P78 – P82 at T_H = 170 °C, v_{PH} = 50 mm/s, w_E = 1.9 mm and M = 0.1 mm. The mean value of the density is $\rho_E \approx$ 118 kg/m^3 with a standard deviation of approx. 6.4 %. The average of the actual extrusion width is $w_{E,m} \approx$ 1.86 mm with a standard deviation of approx. 2.8 %, the measured average layer height $h_{E,m} \approx$ 1.82 mm with a standard deviation of approx. 0.7 %. This means that the values of $w_{E,m}$ and $h_{E,m}$ are lower overall than the specified 1.9 mm, but are only subject to minor fluctuations. The density is exposed to somewhat greater fluctuations. This may be due to non-uniform blowing agent

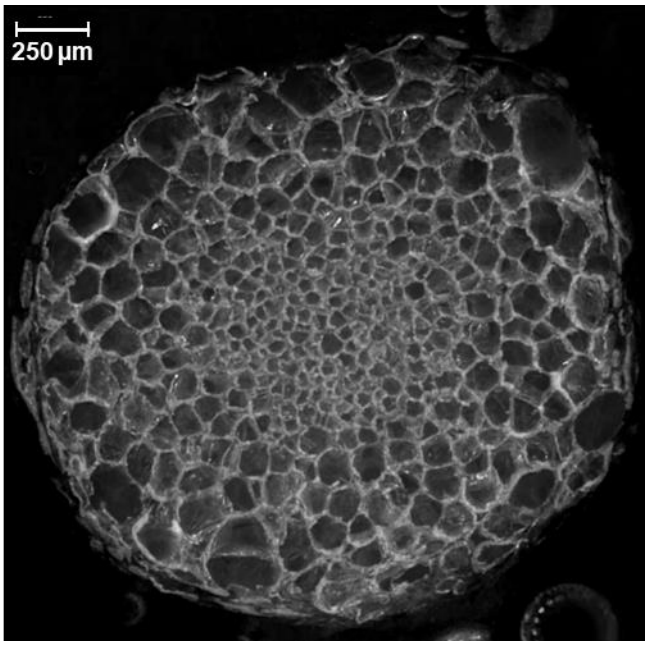

Figure 8: Optical microscope image of the cross section of the extruded strand printed with P35 parameters

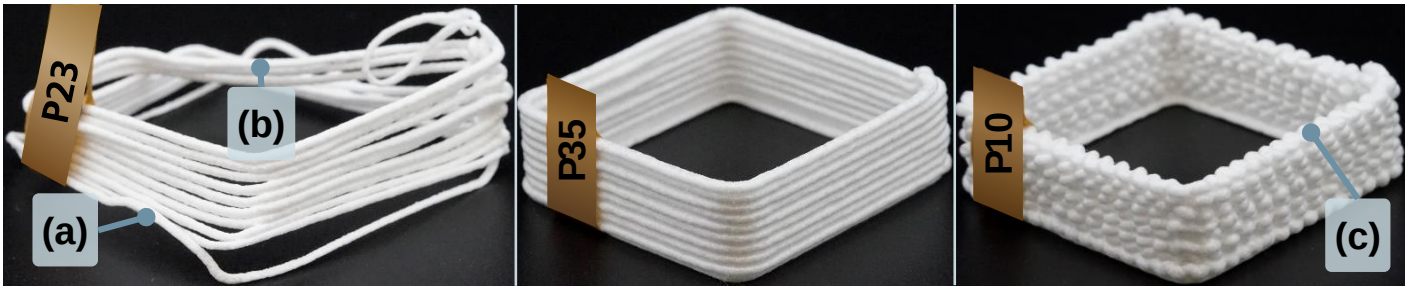

Figure 7: Printed foam test parts of poor (left and right) and good (middle) quality: (a) no print bed adhesion; (b) material carried over due to under-extrusion; (c) material lateral evasion due to over-extrusion

distribution in the filament and the different densities in different test part areas. The mean values mentioned are summarised below as the result for test P88. Three different scenarios for interpretation are explained with the aim of finding suitable parameter sets.

Scenario 1 analyses the influence of the print head velocity v_{PH} on the print result. The tests P01, P19, P20, P27 – P37, P88 are considered here, where T_H = 170 °C is constant. w_E is analysed in two configurations at 1.65 mm and 1.9 mm and M at 0.1 and 0.11. v_{PH} is varied between 50 mm/s and 75 mm/s in 5 mm/s steps. The density distribution over the print head velocity is shown in Figure 9. No adhesion could be achieved at higher v_{PH} and therefore these cannot be analysed. At w_E = 1.9 mm, ρ_E increases steeply over v_{PH} and here also due to the constant M over v_F, which agrees with the results from the extrusion tests. The earlier print error at w_E = 1.9 mm can be explained by a smaller v_F compared to w_E = 1.65 mm. At w_E = 1.65 mm, ρ_E shows no clear tendency. This could be due to the measurement uncertainty of ρ_E. The result of the dimensional measurement via v_{PH} is shown in Figure 10. At w_E = 1.9 mm, $w_{E,m}$ and $h_{E,m}$ drop sharply compared to the target value. This correlates with the increase in ρ_E and suggests that the blowing agent could not be fully activated at high v_F and expansion took place to a lesser extent. $w_{E,m}$ and $h_{E,m}$ show no clear trend at w_E = 1.65 mm, but are not the same at the respective print head velocity. The deposited cross-section is therefore not round. The change from $w_{E,m} > h_{E,m}$ to $w_{E,m} < h_{E,m}$ at $v_{PH} \approx 58$ mm/s can be interpreted as a change from a lateral over-extrusion to an under-extrusion. Considering the model from Figure 2 this could mean that a change from $v_{PH} < v_I$ to $v_{PH} > v_I$ takes place here.

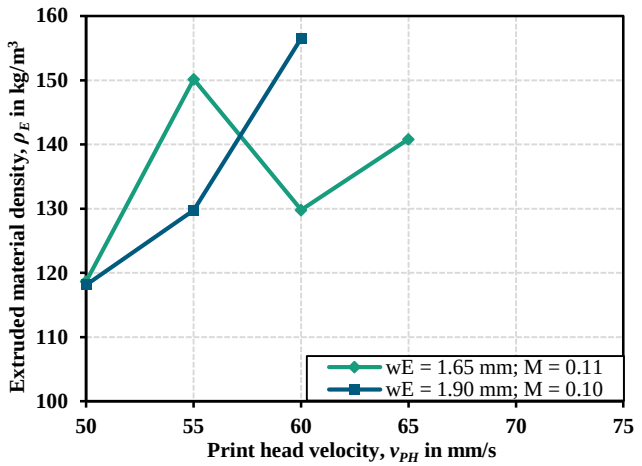

Figure 9: Scenario 1: extruded material density ρE as a function of print head velocity vPH at two different extrusion widths wE and Multipliers M

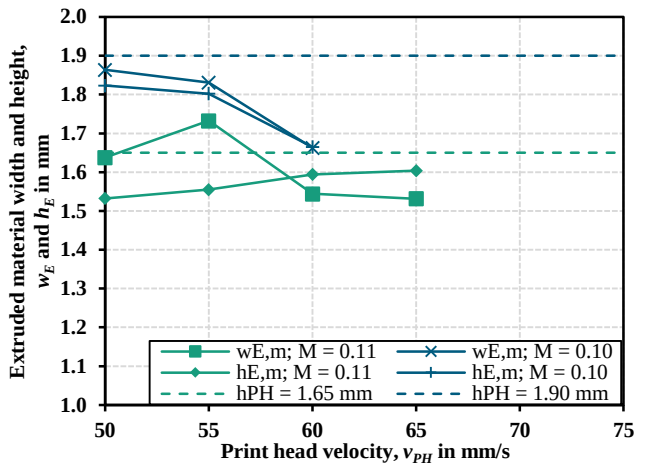

Figure 10: Scenario 1: extruded material width $w_{E,m}$ and height $h_{E,m}$ as a function of print head velocity v_{PH} at two different print heights h_{PH} (dashed lines) and Multipliers M

Scenario 2 considers experiments P82 – P87. There, T_H = 170 °C, v_F = 7.5 mm/s and M = 0.1 is constant. v_{PH} is changed from 50 mm/s to 75 mm/s in 5 mm/s steps and w_E is changed from 1.9 mm to 1.55 mm in accordance with the definition in Eq. (4). The resulting ρ_E is plotted against w_E in Figure 11. With increasing w_E, ρ_E tends to increase. This corresponds to the opposite of scenario 1, in which increasing v_{PH} also resulted in lower ρ_E. However, with a difference of $\Delta\rho_E \approx 14$ kg/m^3 over the v_{PH} range,

the effect is much smaller than the difference $\Delta\rho_E \approx 38$ kg/m^3 in scenario 1. The constant v_F results in a more constant ρ_E than a constant w_E. In other words, a good processing window is found here for the aim of a low density over different v_{PH} values. The comparison of $w_{E,m}$ and $h_{E,m}$ with the set extrusion width w_E shows that this was achieved in the height $h_{E,m}$, but initially not in the width $w_{E,m}$ (Figure 12). This means that, as initially assumed, the extruded cross-section is more rectangular at low h_{PH} and thus w_E. With the simultaneously high v_{PH} and low v_F, it is possible that not enough material is extruded. However, since ρ_E is comparatively very low, it is assumed that $v_I \approx v_{PH}$. This is because when v_{PH} decreases, i.e. $v_{PH} < v_I$, $w_{E,m}$ increases relative to $h_{E,m}$ until it exceeds w_E = 1.9 mm and over-extrusion occurs.

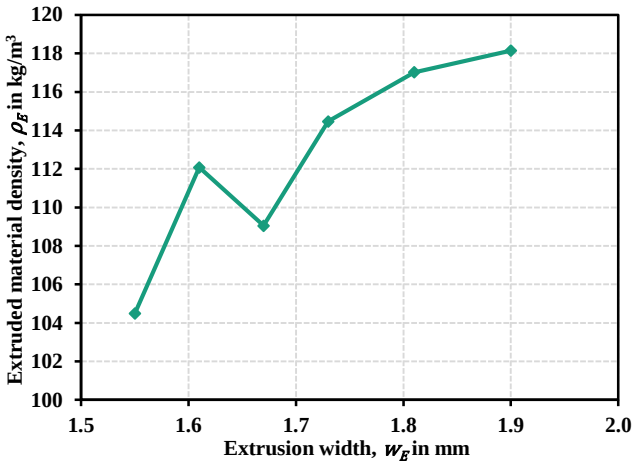

Figure 11: Scenario 2: extruded material density ρE as a function of extrusion width wE,m

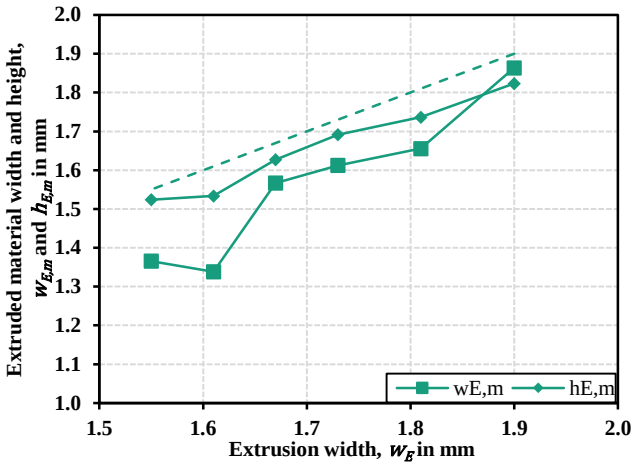

Figure 12: Scenario 2: extruded material width wE,m and height hE,m as a function of extrusion width wE (dashed lines)

Scenario 3 shows the selection of tests P01, P05, P35 – P42. v_{PH} = 50 mm/s constant, v_F at 6.2 mm/s and 7.5 mm/s, h_{PH} at 1.65 mm and 1.9 mm and M at 0.1 and 0.11 for two configurations, T_H = 160 – 180 °C in 5 °C steps are considered. The result for ρ_E is shown in Figure 13. As with the extrusion tests, ρ_E is lowest at low T_H. The almost equal ρ_E at the respective T_H indicates a strong effect of the calculation of the set parameters with Eq. (4) on ρ_E relatively independent of the temperature. A difference is only observed at T_H = 180 °C. Figure 14 could provide information on this. The measured, averaged layer height $h_{E,m}$ and the measured extrusion width $w_{E,m}$ decrease with increasing T_H. At h_{PH} = 1.65 mm, $h_{E,m}$ is usually lower than $w_{E,m}$. All other parameters being equal, this could mean a collapse of the paths caused by the temperature, which in turn corresponds with the experience from the extrusion tests. At h_{PH} = 1.65 mm, the difference between $h_{E,m}$ and $w_{E,m}$ is greater than at h_{PH} = 1.9 mm. This indicates over-extrusion and therefore $v_{PH} < v_I$ may always apply. As the set width w_E is reached at low T_H ($w_{E,m} \approx w_E$), it is assumed that the low h_{PH} leads to a reduction in $h_{E,m}$. At higher T_H, the collapse of the material probably predominates.

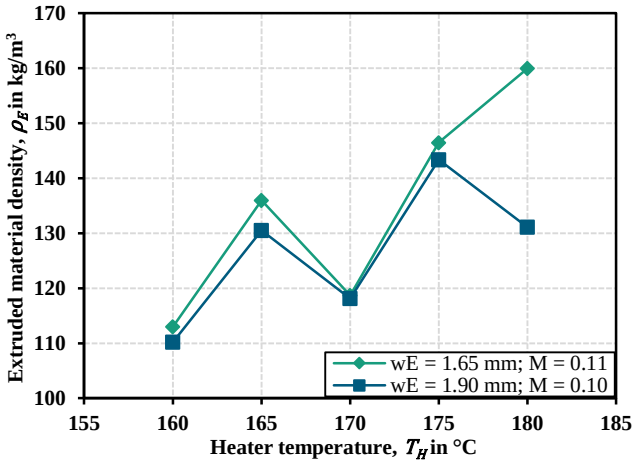

Figure 13: Scenario 3: extruded material density ρ_E as a function of heater temperature T_H at two different extrusion widths w_E and Multipliers M

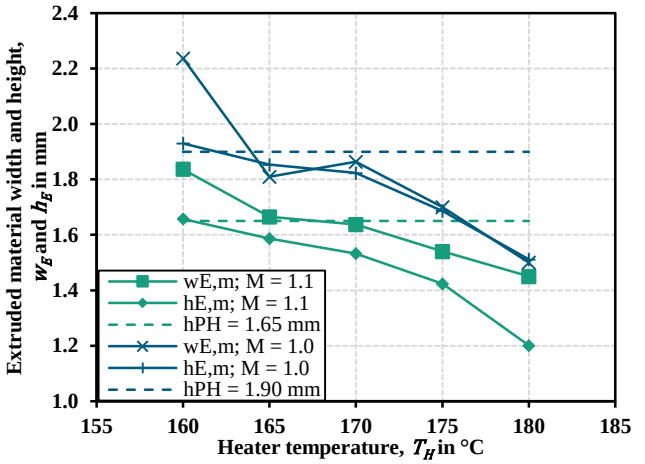

Figure 14: Scenario 3: extruded material width $w_{E,m}$ and height $h_{E,m}$ as a function of heater temperature T_H at two different print heights h_{PH} (dashed lines) and Multipliers M

Conclusion and outlook

With the help of a new method of loading thermoplastic filaments with a physical blowing agent, it was shown that polymer foam components with a low density of approx. 105 kg/m³ can be produced using FFF. Suitable parameters for use in the printer were found by studying the properties during extrusion. A parameter study with an FFF printer made it possible to analyse the relationships between printing temperature, feeding velocity, print head velocity, print head height, extrusion width and multiplier. This made it possible to identify suitable parameter combinations supported by a calculation model.

In the future, larger investigations, e.g. by means of Design of Experiments (DoE), will be necessary for an even more precise investigation of the processing window. In addition, the influence of the selected parameters on pore size and mechanical properties must be analysed. This will also allow the poor adhesion of the extruded material paths to each other, which is assumed due to the circular cross-section, to be verified.

Acknowledgement

The results were obtained within the project „IBÖM03: bioxXprint - der Bio-Schaum-Drucker für gradierte Strukturen“ (Funding reference number: 03180860C), that was founded by the German Federal Ministry of Education and Research (BMBF). The project was led by the “Institut für Holztechnologie Dresden gemeinnützige GmbH”. The author would like to thank the sponsor for founding the project and the project partners for the professional and successful collaboration.

Literatur

[1] J. Zheng und S. Suh, "Strategies to reduce the global carbon footprint of plastics," *Nat. Clim. Chang.*, Jg. 9, Nr. 5, S. 374–378, 2019, doi: 10.1038/s41558-019-0459-z.

[2] I. D. Posen, P. Jaramillo und W. M. Griffin, "Uncertainty in the Life Cycle Greenhouse Gas Emissions from U.S. Production of Three Biobased Polymer Families," *Environmental science & technology*, Early Access. doi: 10.1021/acs.est.5b05589.

[3] F.-L. Jin, M. Zhao, M. Park und S.-J. Park, "Recent Trends of Foaming in Polymer Processing: A Review," *Polymers*, Early Access. doi: 10.3390/polym11060953.

[4] V. Dhokia und S. Newman, "The design and manufacture of individualised perfect-fit packaging," in *ICED15, The 20th International Conference on Engineering Design*, Milan, Italy, Christian Weber, Stephan Husung, Marco Cantamessa, Gaetano Cascini, Dorian Marjanovic, Monica Bordegoni, Hg., 2015.

[5] M. Nofar, J. Utz, N. Geis, V. Altstädt und H. Ruckdäschel, "Foam 3D Printing of Thermoplastics: A Symbiosis of Additive Manufacturing and Foaming Technology," *Advanced Science*, Jg. 9, Nr. 11, S. 2105701, 2022, doi: 10.1002/advs.202105701.

[6] J. Martínez, J. Dumas und S. Lefebvre, "Procedural voronoi foams for additive manufacturing," *ACM Trans. Graph.*, Jg. 35, Nr. 4, 2016, Art. Nr. 44, doi: 10.1145/2897824.2925922.

[7] M. J. Prajapati, A. Kumar, S.-C. Lin und J.-Y. Jeng, "Multi-material additive manufacturing with lightweight closed-cell foam-filled lattice structures for enhanced mechanical and functional properties," *Additive Manufacturing*, Jg. 54, S. 102766, 2022, doi: 10.1016/j.addma.2022.102766.

[8] B. H S, D. Bonthu, P. Prabhakar und M. Doddamani, "Three-Dimensional Printed Lightweight Composite Foams," *ACS omega*, Early Access. doi: 10.1021/acsomega.0c03174.

[9] A. Pawar, G. Ausias, Y.-M. Corre, Y. Grohens und J. Férec, "Mastering the density of 3D printed thermoplastic elastomer foam structures with controlled temperature," *Additive Manufacturing*, Jg. 58, S. 103066, 2022, doi: 10.1016/j.addma.2022.103066.

[10] K. Kalia, B. Francoeur, A. Amirkhizi und A. Ameli, "In Situ Foam 3D Printing of Microcellular Structures Using Material Extrusion Additive Manufacturing," *ACS Appl Mater Interfaces*, Early Access. doi: 10.1021/acsami.2c03014.

[11] V. Kakumanu und S. Srinivas Sundarram, "Dual pore network polymer foams for biomedical applications via combined solid state foaming and additive manufacturing," *Mater Lett*, Jg. 213, S. 366–369, 2018, doi: 10.1016/j.matlet.2017.11.027.

[12] M. Zhou, M. Li, J. Jiang, N. Gao, F. Tian und W. Zhai, "Construction of Bionic Porous Polyetherimide Structure by an In Situ Foaming Fused Deposition Modeling Process," *Adv Eng Mater*, Jg. 24, Nr. 3, 2022, Art. Nr. 2101027, doi: 10.1002/adem.202101027.

[13] M. G. M. Marascio, J. Antons, D. P. Pioletti und P.-E. Bourban, "3D Printing of Polymers with Hierarchical Continuous Porosity," *Adv Materials Technologies*, Jg. 2, Nr. 11, 2017, Art. Nr. 1700145, doi: 10.1002/admt.201700145.

[14] R. Dugad, G. Radhakrishna und A. Gandhi, "Solid-state foaming of acrylonitrile butadiene styrene through microcellular 3D printing process," *Journal of Cellular Plastics*, Jg. 58, Nr. 2, S. 325–355, 2022, doi: 10.1177/0021955X211009443.

[15] M. Zhou, B. Chen, Y. Li, J. Jiang und W. Zhai, "Enhanced Interfacial Adhesion and Increased Isotropy of 3D Printed Parts with Microcellular Structure Fabricated via a

Micro-Extrusion CO 2 -Foaming Process," *Adv Eng Mater*, Jg. 25, Nr. 8, 2023, Art. Nr. 2201468, doi: 10.1002/adem.202201468.
[16] T. Standau, C. Zhao, S. Murillo Castellón, C. Bonten und V. Altstädt, "Chemical Modification and Foam Processing of Polylactide (PLA)," *Polymers*, Early Access. doi: 10.3390/polym11020306.
[17] R. Comminal, M. P. Serdeczny, D. B. Pedersen und J. Spangenberg, "Numerical modeling of the strand deposition flow in extrusion-based additive manufacturing," *Additive Manufacturing*, Jg. 20, S. 68–76, 2018, doi: 10.1016/j.addma.2017.12.013.
[18] M. Mihai, M. A. Huneault, B. D. Favis und H. Li, "Extrusion foaming of semi-crystalline PLA and PLA/thermoplastic starch blends," *Macromolecular bioscience*, Jg. 7, Nr. 7, S. 907–920, 2007, doi: 10.1002/mabi.200700080.
[19] J. Fischer, M. Echsel, P. Springer und O. Refle, "In-line measurement of extrusion force and use for nozzle comparison in filament based additive manufacturing," *Progress in Additive Manufacturing*, Jg. 8, S. 9–17, 2023, doi: 10.1007/s40964-022-00385-5.

Kontaktangaben

Dipl.-Ing. Patrick Springer
Fraunhofer-Institut für Produktionstechnik und Automatisierung IPA
Nobelstraße 12 │ 70569 Stuttgart
Telefon +49 711 970-1996
E-Mail: patrick.springer@ipa.fraunhofer.de
WEB: www.ipa.fraunhofer.de

Appendix

Table 1: Test plan foam extrusion

No.	Heater temperature T_H in °C	Feeding velocity v_F in mm/s
E01	160	3
E02	160	4.5
E03	160	6
E04	160	7.5
E05	160	9
E06	160	12
E07	170	3
E08	170	4.5
E09	170	6
E10	170	7.5
E11	170	9
E12	170	12
E13	180	3
E14	180	4.5
E15	180	6
E16	180	7.5
E17	180	9
E18	180	12

No.	Heater temperature T_H in °C	Feeding velocity v_F in mm/s
E18	190	3
E19	190	4.5
E20	190	6
E21	190	7.5
E22	190	9
E23	190	12
E24	200	3
E25	200	4.5
E26	200	6
E27	200	7.5
E28	200	9
E29	200	12
E30	210	9
E31	210	12
E32	220	9
E33	220	12
E34	230	9
E35	230	12

Table 2: Test plan foam printing

No.	Heater temperature T_H in °C	Print velocity v_{PH} in mm	Feeding velocity v_F in mm/s	Print height h_{PH} in mm	Multiplier M
P01	170	50	6.2	1.65	0.11
P02	170	50	7.4	1.65	0.13
P03	170	50	9.1	1.65	0.16
P04	170	50	6.0	1.9	0.08
P05	170	50	7.5	1.9	0.1
P06	170	50	9.0	1.9	0.12
P07	170	50	5.8	2.15	0.06
P08	170	50	7.7	2.15	0.08
P09	170	50	8.6	2.15	0.09
P10	170	25	5.9	1.65	0.21
P11	170	25	7.9	1.90	0.21
P12	170	25	9.2	2.05	0.21
P13	170	75	5.9	1.65	0.07
P14	170	75	7.9	1.90	0.07
P15	170	75	9.2	2.05	0.07
P16	170	62.5	5.7	1.65	0.08
P17	170	62.5	7.5	1.90	0.08
P18	170	62.5	8.7	2.05	0.08
P19	170	55	6.8	1.65	0.11
P20	170	55	8.3	1.90	0.1
P21	170	62.5	7.8	1.65	0.11
P22	170	62.5	9.4	1.90	0.1
P23	170	50	5.1	1.65	0.09
P24	170	50	6.0	1.90	0.08
P25	170	50	4.0	1.65	0.07
P26	170	50	4.5	1.90	0.06
P27	170	60	7.5	1.65	0.11
P28	170	65	8.1	1.65	0.11
P29	170	70	8.7	1.65	0.11
P30	170	75	9.3	1.65	0.11
P31	170	60	9.0	1.90	0.1
P32	170	65	9.8	1.90	0.1
P33	170	70	10.5	1.90	0.1
P34	170	75	11.3	1.90	0.1
P35	160	50	6.2	1.65	0.11
P36	160	50	7.5	1.90	0.1
P37	165	50	6.2	1.65	0.11
P38	165	50	7.5	1.90	0.1
P39	175	50	6.2	1.65	0.11
P40	175	50	7.5	1.90	0.1
P41	180	50	6.2	1.65	0.11
P42	180	50	7.5	1.90	0.1
P43	180	50	5.1	1.49	0.11
P44	180	50	6.1	1.71	0.1
P45	180	50	5.1	1.65	0.09
P46	180	50	6.0	1.90	0.08
P47	180	50	6.1	1.57	0.12
P48	180	50	7.5	1.81	0.11
P49	180	50	6.0	1.49	0.13
P50	180	50	7.3	1.71	0.12
P51	180	50	7.6	1.62	0.14
P52	180	50	7.7	1.52	0.16
P53	180	50	7.7	1.43	0.18
P54	180	50	7.4	1.33	0.2
P55	180	55	8.0	2.09	0.08
P56	180	55	7.3	2.00	0.08
P57	180	55	7.4	1.90	0.09
P58	180	55	7.5	1.81	0.1
P59	180	55	7.4	1.71	0.11
P60	180	55	7.2	1.62	0.12
P61	180	55	7.4	1.52	0.14
P62	180	55	7.5	1.43	0.16
P63	180	60	7.3	1.71	0.1
P64	180	60	7.2	1.62	0.11
P65	180	60	7.5	1.52	0.13
P66	180	60	7.7	1.43	0.15
P67	175	50	6.1	1.57	0.12
P68	175	50	6.0	1.49	0.13
P69	175	55	7.5	1.81	0.1
P70	175	55	7.4	1.71	0.11
P71	170	50	5.7	1.65	0.1
P72	170	50	7.5	1.90	0.1
P73	170	50	8.7	2.05	0.1
P74	185	65	7.5	1.52	0.12
P75	185	65	7.7	1.43	0.14
P76	190	70	7.7	1.43	0.13
P77	190	70	7.7	1.33	0.15
P78	170	50	7.5	1.90	0.1
P79	170	50	7.5	1.90	0.1
P80	170	50	7.5	1.90	0.1
P81	170	50	7.5	1.90	0.1
P82	170	50	7.5	1.90	0.1
P83	170	55	7.5	1.81	0.1
P84	170	60	7.5	1.73	0.1
P85	170	65	7.5	1.67	0.1
P86	170	70	7.5	1.61	0.1
P87	170	75	7.5	1.55	0.1
P88	170	50	7.5	1.90	0.1

Table 3: Overall results foam printing

No.	Extruded material density, ρ_E in kg/m³	Extruded material width w_E	Actual part height P_H	Extruded material height h_E
P01	136.5	1.64	14.62	1.53
P02	118.7	1.89	15.43	1.62
P03	151.4	2.11	16.22	1.71
P04	155.6	1.43	11.49	1.32
P05	127.8	1.89	15.46	1.81
P06	150.8	2.04	16.11	1.89
P07	172.5	1.39	8.85	1.11
P08	124.0	1.87	13.91	1.83
P09	148.3	1.99	14.87	1.97
P10	140.2	3.52	15.51	1.63
P11	119.2	4.87	17.48	2.07
P12	113.7	5.58	17.08	2.29
P13	187.8	1.30		
P14	123.9	1.56	13.62	1.58
P15				
P16	129.4	1.32		
P17	126.8	1.73	13.55	1.58
P18				
P19	150.2	1.73	14.82	1.56
P20	129.8	1.83	15.37	1.80
P21	131.1	1.73	15.57	1.64
P22				
P23	282.1	1.20		
P24	145.2	1.45	12.16	1.40
P25				
P26				
P27	129.8	1.54	15.17	1.59
P28	140.8	1.53	15.26	1.60
P29				
P30				
P31	156.6	1.66	14.27	1.66
P32				
P33				
P34				
P35	113.0	1.84	15.74	1.66
P36	110.2	2.24	16.39	1.93
P37	136.0	1.67	15.10	1.59
P38	130.5	1.81	15.78	1.85
P39	146.5	1.54	13.64	1.42
P40	143.4	1.70	14.44	1.69
P41	160.0	1.45	11.63	1.20
P42	131.1	1.50	13.04	1.51
P43	161.2	1.16		
P44	153.7	1.45	12.73	1.32
P45	240.5	1.14		
P46	176.2	1.38	11.43	1.31
P47	166.6	1.41	14.42	1.36
P48	145.7	1.55	13.30	1.55
P49	167.3	1.40	14.12	1.34
P50	135.6	1.59	14.43	1.51
P51	150.2	1.64	14.99	1.58
P52	141.5	1.66	15.54	1.48
P53	149.3	1.67	16.41	1.43
P54	135.6	1.58	16.46	1.32
P55	123.3	1.60	12.01	1.57
P56	139.4	1.59	12.13	1.39
P57	146.9	1.50	13.19	1.53
P58	135.7	1.51	13.64	1.59
P59	144.5	1.58	14.72	1.54
P60	149.6	1.53	14.09	1.48
P61	140.5	1.39	14.79	1.40
P62	126.1	1.53	15.81	1.37
P63	144.7	1.53	13.10	1.36
P64	152.2	1.52	14.05	1.47
P65	138.2	1.55	15.24	1.45
P66	145.3	1.54	15.93	1.38
P67	166.4	1.43	14.71	1.39
P68	175.3	1.35	14.07	1.33
P69	127.7	1.49	13.24	1.54
P70	146.4	1.49	15.10	1.58
P71	164.2	1.44	13.40	1.40
P72	123.8	1.89	15.55	1.83
P73	146.8	2.06	14.63	1.94
P74	144.3	1.98	14.53	1.38
P75	131.8	1.57	15.83	1.37
P76	135.0	1.49	16.08	1.40
P77	131.6	1.44	16.33	1.31
P78	114.0	1.88	15.40	1.81
P79	115.1	1.95	15.74	1.85
P80	111.2	1.84	15.55	1.82
P81	109.1	1.81	15.53	1.82
P82	126.2	1.79	15.52	1.82
P83	117.0	1.66	14.80	1.74
P84	114.5	1.61	16.09	1.69
P85	109.1	1.57	15.48	1.63
P86	112.1	1.34	14.61	1.53
P87	104.5	1.37	16.01	1.52
P88	118.2	1.86	15.54	1.82